ACS OMEGA

Open Access

http://pubs.acs.org/journal/acsodf

Article

Assessing CO_2 Adsorption Behavior onto Free-Standing, Flexible Organic Framework-PVDF Composite Membrane: An Empirical Modeling and Validation of an Experimental Data Set

Hridoy Jyoti Bora, Reetesh Borpatra Gohain, Pranjal Barman, Subir Biswas, Neelotpal Sen Sarma, and Anamika Kalita*

Cite This: *ACS Omega* 2023, 8, 36065−36075

Read Online

ACCESS | Metrics & More | Article Recommendations | Supporting Information

ABSTRACT: Covalent organic framework (COF) materials have greatly expanded their range in a variety of applications since the cognitive goal of a highly organized and durable adsorbent is quite rational. The characteristics of a conjugated organic framework are combined with an industrially relevant polymer to produce a composite membrane optimized for selectively adsorbing carbon dioxide (CO_2) gas across a wide temperature range. Additionally, treatment of the composite membrane with cold atmospheric plasma (CAP) that specifically enhanced the parent membrane's surface area by 36% is established. Following CAP treatment, the membrane accelerates the CO_2 uptake by as much as 66%. This is primarily due to a Lewis acid−base interaction between the electron-deficient carbon atom of CO_2 and the newly acquired functionalities on the COFs@PVDF membrane's surface. In particular, the C−N bonds, which appear to be a higher electron density site, play a key role in this interaction. Moreover, the empirical model proposed here has confirmed CO_2 adsorption phenomena in the COF@PVDF composite membrane, which closely matches the findings from the experimental data set under designated operating conditions. As a result, the current study may pave the way for future design work as well as refine the covalent framework polymer composite membrane's features, revealing a more sophisticated approach to addressing CO_2 capture problems.

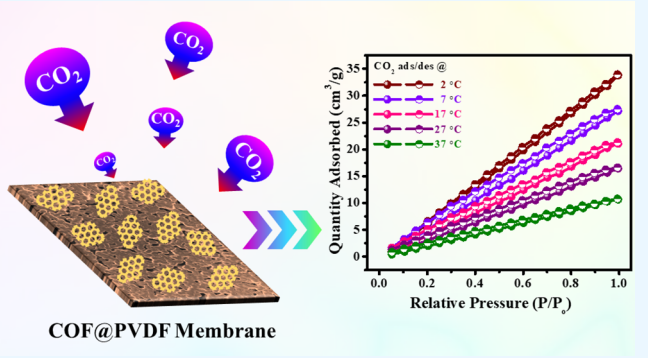

INTRODUCTION

There has been advancement in industrialization, but human activities have accentuated the escalating production of carbon dioxide (CO_2) in the atmosphere, which intensifies the global temperature and can cause serious environmental complications that will confront mankind in the future.[1,2] Management and abatement of greenhouse gases, due to their influence on biodiversity, climate change, agriculture, and so forth,[3] have attracted the attention of the scientific community; a more cutting-edge strategy, including negative emission technology, is required. Several methods have been established to effectively alleviate the harmful impacts of CO_2, such as fractionation, membrane separation, solvent scrubbing, and so on,[4,5] where adsorption, due to its simplicity and low cost, has a great assurance to attenuate such environmental toxins.[6,7] Nevertheless, a variety of adsorbents appear to be proficient in removing these toxins,[8−10] but covalent organic frameworks (COFs) stand out as the materials that have the greatest potential of effectively capturing CO_2. The porous 2D/3D crystalline COFs are receiving a lot of interest owing to their remarkable potential, exclusively in the domain of gas collection and separation[11−13]. COFs have been highlighted as ideal candidates for CO_2 capture due to their high CO_2 uptake, excellent CO_2 selectivity, repeated use, ease of pore surface engineering, ordered pore distribution, low energy penalty for regeneration, good stability, predetermined structures, high structural varieties, rich porosities, and structural and chemical tunability. Some COFs, in particular, may be used frequently and consecutively while still performing well at capturing CO_2 in humid conditions.[14,15] COFs are made of organic subunits bonded together by strong covalent bonds, which also improves stability.[16,17] Liable to the structural flexibility and tunability, COFs can extend a compatible platform for designing mutable efficient materials to realize multiple demands.[18−22]

Countless attempts have been made in recent years to engineer polymeric or derived polymeric composite materials that possess excellent CO_2 adsorption attributes. In this regard,

Received: June 13, 2023
Accepted: September 11, 2023
Published: September 22, 2023

Scheme 1. Schematic Representation for the Fabrication of COF@PVDF Support

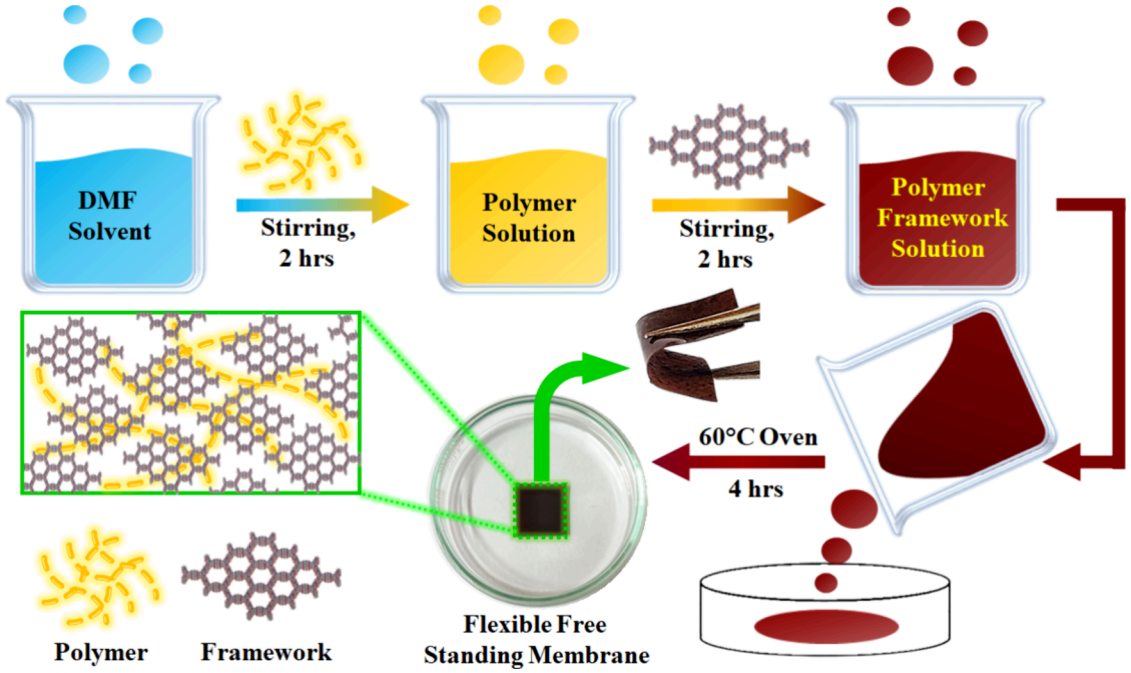

there is a rising interest in exploring the avenues of polymer-COF membranes, since COFs, due to their astounding property of organic coordination framework, offer enhanced processability and compatibility to be employed as membrane materials with varied polymers.[23−26] COF-membranes have been assessed for their usefulness in energy storage, water purification, biofuel generation, and other fields,[27−31] and it is projected that the field of membrane technology will increase in the next years. Many techniques for fabricating COF membranes have been investigated, including solvothermal, interfacial polymerization, layer-by-layer stacking, and so on,[32−34] but the demand for simple and active production methods is still unmet. While the inspection for the facile fabrication procedure is advancing, numerous postfurnishing modification methods strongly affect the topology and hence the properties of the framework membranes.

As a result, contemporary research has focused on the creation of organic framework−polymer composite membranes with multifunctional activity, such as superior surface characteristics, remarkable adsorption performances, and so on, using a variety of synthesis and postmodification techniques. In this regard, we established a simple and cost-effective approach for constructing COF-membranes on poly(vinylidene fluoride) (PVDF) polymer support (COF@PVDF) in this study. PVDF has been widely studied for a variety of applications due to its great chemical stability in harsh environments and robust mechanical properties.[35] Here, for the first time, we have used a revolutionary one-step technology, viz., cold atmospheric plasma (CAP)[36] treatment to postfurnish the membranes for the successful adsorption of CO_2 gas. The COF@PVDF membranes that have undergone CAP plasma treatment exhibit an increase in surface area, which, when compared to the parent membrane, increases the efficacy of CO_2 adsorption. To the best of our knowledge, no reports have yet been published that create a postfurnishing methodology, that is, CAP, on the composite membrane that allows for an advanced efficacy of CO_2 uptake by 66% compared to the pristine one. An additional proposed empirical modeling is also presented here to confirm the CO_2 adsorption phenomena in the COF@PVDF composite membrane under designated operating conditions.

MATERIALS AND METHODS

Poly(vinylidene fluoride) (PVDF) (Sigma-Aldrich) and *N*,*N*′-dimethylformamide (DMF) (Merck) were purchased and used as is. All additional reagents used were of analytical grade. Powder X-ray diffraction (PXRD) analysis was performed on a Bruker AXS instrument (Model D8 Advance). Thermal gravimetric analysis (TGA) was performed on a Mettler Toledo TGA instrument (Model TG/SDTA 851e). A SIGMA VP (ZEISS) field emission scanning electron microscope was used for recording the morphological textures. An Autosorb iQ MP-AG (2 STAT) Anton Paar BET analyzer was used to carry out BET surface area, pore volume, and CO_2 adsorption measurements. Atomic force microscopy (Model No. NTEGRA Vita from NT-MDT) was used to measure the surface roughness. A KRUSS contact angle analyzer (DSA30E) was used to record the sample's wettability using the sessile drop method. ATR measurements were conducted on a PerkinElmer Spectrum-Two. The Vesta program was used to extract the molecular structure of the studied compound. X-ray photoelectron spectroscopy (XPS) analysis was carried out on an ESCALAB Xi+ (Thermo Fischer Scientific Pvt. Ltd., UK).

Synthesis of COF. The synthetic procedure and the detailed characterization of the pristine COF were presented in our previous report.[37] A straightforward hydrothermal reaction process was used for the production of COF. A mixture of NTCDA (100.5 mg, 0.37 mmol) and TAPA (72.5 mg, 0.25 mmol) was sonicated for 5 min in 10 mL of anhydrous DMF. Following that, the mixture was transferred to the appropriate Teflon-lined autoclave reactor (50 mL), permitting the hydrothermal treatment at 180 °C for a time period of 1 day, named COF. The as-synthesized precipitates were thoroughly washed with a large volume of low surface tension

https://doi.org/10.1021/acsomega.3c04198
ACS Omega 2023, 8, 36065−36075

solvents, such as EtOH, and finally with *n*-hexane for 3 days in order to obtain the activated COF. This was carried out since the surface tension of solvents seems to be an important consideration in the activation process of COFs and, consequently, the surface properties. The yield was 89.1%.

Synthesis of COF@PVDF Support. At first, to prepare the PVDF-supported COF membranes, i.e., COF@PVDF, an optimized solution of 7 wt % PVDF was prearranged by mixing the desired quantity of PVDF in DMF solvent under continuous stirring and heating at 60 °C. Different loading ratios of powdered COF,[37] viz., 10, 30, 50, and 80 mg, were mixed with the prepared PVDF solution separately to obtain COF@PVDF support, marked as M-10, M-30, M-50, and M-80, respectively. After ensuring the homogeneous mixing, a simple casting procedure was followed and kept in an oven at 60 °C for 4 h to obtain the desired flexible, free-standing membranes for further investigations.

Cold Atmospheric Plasma Treatment. Cold atmospheric plasma (CAP) was used to treat the composite membranes.[36] CAP was produced by delivering a high-voltage pulse between two electrodes. One of the electrodes is shaped like a cylinder and has a thin coating of dielectric material on it. The other electrode is electrically grounded and has a planner-like form. The film was held on a borosilicate petri dish of diameter Φ = 50 mm, which was placed on the grounded electrode by keeping an air gap of 1.5 mm from the high-voltage electrode. CAP is obtained by applying a high voltage of amplitude 23−25 kV between the electrodes. In order to achieve the optimal condition, different durations of treatment time by considering 23 kV of voltage are allotted on the chosen membrane, such as 0.5, 1, 3, and 5 min, to acquire plasma-treated M-0.5, M-1, M-3, and M-5 membranes, along with different amplitudes of voltage by setting the time to 3 min, such as 24 and 25 kV, termed MV-24 and MV-25, respectively.

Carbon Dioxide Uptake Study. For the CO_2 uptake study, the as-fabricated composite membranes were placed in the BET instrument's degassing chamber and allowed to degas for 2 h at 300 °C. After degassing, the membranes were transferred to an analysis chamber outfitted with CO_2 uptake accessories, and the CO_2 adsorption analysis was performed at various temperatures, including 2, 7, 17, 27, and 37 °C, with the relative pressure regulated at 0 to 1 bar. The gas injection rate into the BET instrument was set to 10 psi or 0.7 kg/cm^2 per min.

RESULTS AND DISCUSSION

The synthetic procedure and the detailed characterization of the pristine COF were presented in our previous report.[37] As shown in Scheme 1, different loading ratios of pristine-COF mixed with an optimized concentration of 7 wt % PVDF in DMF solutions were taken into consideration for the fabrication of polymer-supported COF membrane, i.e., COF@PVDF, and were denoted as M-0 for the bare PVDF membrane without any loading of COF and M-10, M-30, M-50, and M-80, respectively, for loading of 10, 30, 50, and 80 mg COF, respectively.

The structural properties of all of the fabricated COF@PVDF composite membranes were investigated by using the thin-film mode of XRD, as shown in Figure S1. As displayed, the two peaks at $2\theta \sim 18.6°$ (d = 4.7 Å) and ∼20.2° (d = 4.4 Å), which correspond to the (020) and (110) lattice planes, respectively,[38] signify the characteristic peaks of PVDF, which identifies the crystalline nature of the membrane. Furthermore, with different loading ratios of COF, peaks appear at $2\theta \sim 3.0°$ (d = 29.4 Å), ∼6.4° (d = 13.3 Å), and ∼8.2° (d = 10.7 Å), conforming to the (100), (200), and (210) reflections, respectively, for M-10, 30, 50, and 80 membranes. Notably, a significant enhancement of the peak intensity appears with the increasing loading ratios of the COF material in the polymeric matrix. In addition to this, to illustrate the incorporation of COF on the polymeric matrix, the XRD pattern of M-0 and pristine-COF[37] has also been combined and is presented in Figure S1. In order to verify the thermal stability of the prepared membranes, thermogravimetric analysis (TGA) was investigated, which confirms the thermal stability of the membranes up to 430 °C (Figure S2). The morphological features of all the membranes were assessed via FESEM analysis, as shown in Figure S3a−d, which indicates textured globular networks of the PVDF matrix where the COFs were impregnated on the PVDF surface. The surface properties of all the fabricated membranes were established by BET surface area measurements considering N_2 adsorption−desorption isotherms at 77 K and 1 bar pressure, as shown in Figure S4a, which validates the membranes' intricate porous nature. The analytical findings are given in Table 1, which confirms the microporous nature,[39] as seen in Figure S4b. Figure S3 shows that with the increasing loading ratios of COF, agglomeration takes place over the polymeric membrane. At lower loading ratios, such as M-10 and M-30 membranes, the sample is evenly dispersed in the polymeric matrix, but there may be fewer molecules for adsorption, affecting the membrane's surface area. However, at higher loading ratios, the adsorption process may be limited, i.e., in the case of M-80, due to the formation of agglomeration across the membrane, as compared to M-50, which has a better structural morphology, the acceptable surface area, and the largest pore volume. Therefore, by optimizing COF loading and managing their morphology, surface attributes can be used to their full advantage. Therefore, the M-50 membrane is taken into consideration for further investigations.

Table 1. Summary of Data Presenting the Surface Properties of the Prepared COF@PVDF Support

samples	BET surface area (m^2/g)	pore size (radius) (nm)	total pore volume (cm^3/g)
pristine COF	1428.78	1.527	1.21
M-0	3.73	1.701	0.018
M-10	207.65	1.711	0.188
M-30	311.11	1.717	0.191
M-50	390.56	1.706	0.214
M-80	393.05	1.709	0.208

In continuation with the preferred membrane, Figure 1a,b and c,d corresponds to the digital photographs and FESEM images of the M-0 and M-50 membranes, respectively. The 3D AFM images and the surface roughness profile graphs of M-0 and M-50 membranes are depicted in Figure 1e,f, respectively, where RMS roughness for both membranes was found to be 27.69 and 47.01 nm. Furthermore, the chemical composition of the M-50 membrane was inspected by energy-dispersive X-ray analysis (EDX) that reveals the presence of carbon, nitrogen, oxygen, and fluorine only, as shown in Figure S5.

In recent times, COFs have emerged as an ideal candidate for efficient adsorption of gas molecules. As we all witnessed, the global carbon outpouring has been increasing expeditiously

https://doi.org/10.1021/acsomega.3c04198
ACS Omega 2023, 8, 36065−36075

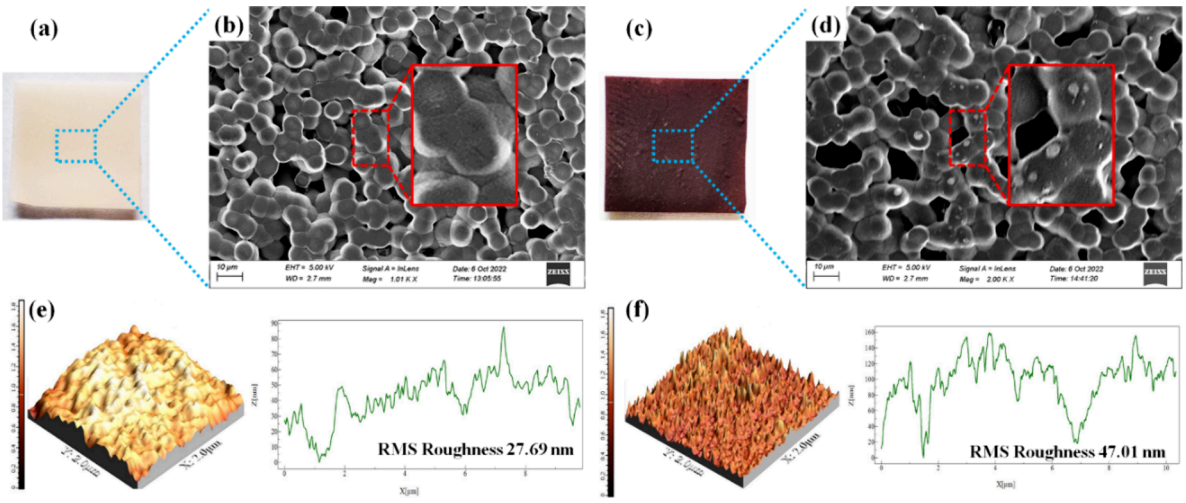

Figure 1. (a, b) and (c, d) Digital photographs and FESEM images of M-0 and M-50 membranes, respectively. (e) and (f) 3D AFM image and roughness profile of M-0 and M-50 membranes, respectively.

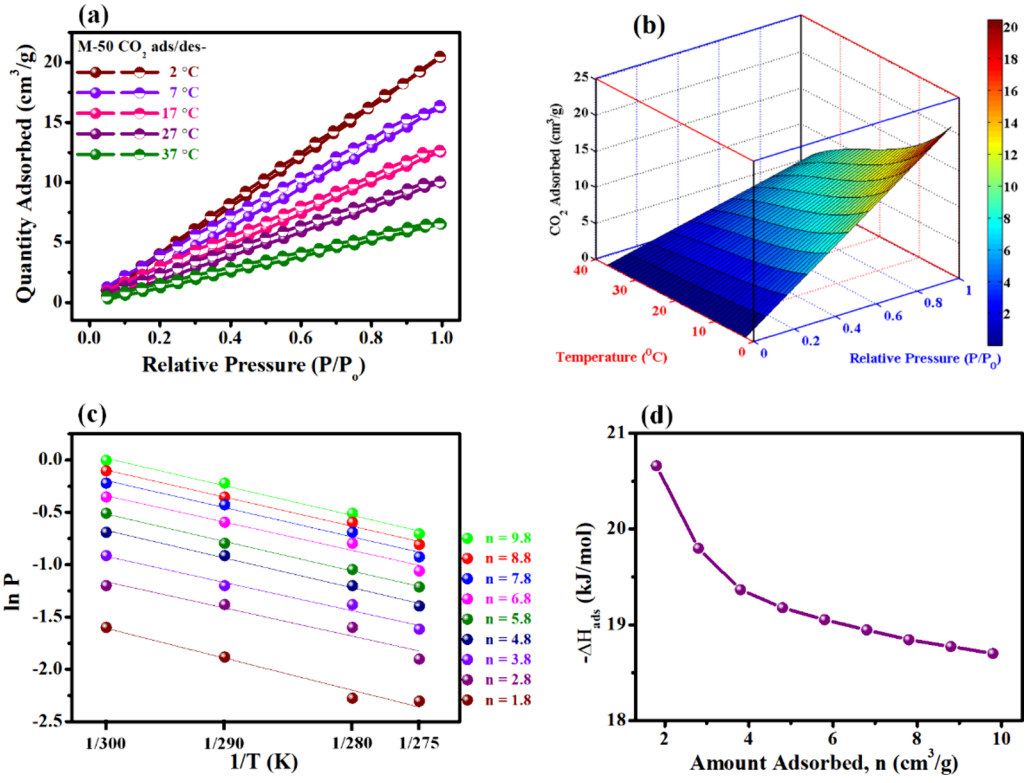

Figure 2. (a) CO_2 adsorption−desorption properties of the M-50 membrane at different temperatures. (b) 3D colormap surface plot representing the amount of CO_2 adsorbed (cm^3/g) against variables such as pressure (bar) and temperature (°C). (c) Isosteric ln p against $1/T$ plot at temperatures 275, 280, 290, and 300 K (2, 7, 17, 27 °C), designed for nine different loadings n (cm^3/g) to illustrate the determination of ΔH_{ads} and (d) isosteric enthalpy of adsorption of CO_2 by the M-50 membrane.

anticipated by the growing demands of energy production and utilizing fossil fuel dominantly for energy supply. In this context, the COF-impregnated polymeric support offers the benefits of cost-effectiveness, effortless fabrication and reusability, and bulk-scale production, along with their built-in features for real-time application. Therefore, to investigate the efficiency of the prepared M-50 membrane toward CO_2 uptake, the adsorption−desorption equilibrium isotherms were examined for a wide range of temperatures, i.e., 2−37 °C and at 1 bar pressure, as shown in Figure 2a. The adsorption of CO_2 on the respective membrane was found to be the highest in the lower temperature range and it decreases with a rise in temperature, such as 20.42 cm^3/g at 2 °C, 16.22 cm^3/g at 7 °C, 12.52 cm^3/g at 17 °C, 9.95 cm^3/g at 27 °C, and 6.51 cm^3/g at 37 °C. The overlapping of adsorption−desorption isotherm curves for all the temperatures and the insignificant hysteresis directly indicates the efficient kinetics and reversible nature of the adsorption−desorption process, i.e., the adsorbed CO_2 gas can be fully recovered after the desorption process on the M-50 membrane. However, in order to elucidate the role of COF on the polymeric matrix, the CO_2 adsorption−desorption isotherm has been checked for the M-0 membrane at ambient

https://doi.org/10.1021/acsomega.3c04198
ACS Omega 2023, 8, 36065−36075

Table 2. Optimized conditions along with surface properties of the plasma-treated M-50 Membrane

sl. no.	name	treatment time (min)	applied voltage (kV)	BET surface area (m^2/g)	enhanced surface area (%)	pore size (radius) (nm)	total pore volume (cm^3/g)
1.	*M-50(w/o treatment)*			*390.56*		*1.706*	*0.214*
2.	M-0.5	0.5	23	418.53	7.16	1.784	0.323
3.	M-1	1	23	487.46	24.81	1.831	0.557
4.	M-3	3	23	532.11	36.24	1.912	0.675
5.	M-5	5	23	536.77	37.43	1.917	0.639
after setting the treatment time to 3 min, varying the applied voltage							
6.	MV-24	3	24	408.98	4.71	1.711	0.338
7.	MV-25	3	25	397.75	1.84	1.697	0.189

temperature, i.e., at 27 °C, it resulted in the adsorption value of only 0.83 cm^3/g, which is negligible as compared to 9.95 cm^3/g for the M-50 membrane, as shown in Figure S6. Moreover, Figure 2b refers to the 3D color mapping of the amount of CO_2 adsorbed on the M-50 membrane concerning different variables, such as pressure and temperature.

In order to explore the potency of the adsorbate and adsorbent's interaction, the isosteric enthalpy of adsorption ($-\Delta H_{ads}$) was estimated from the isotherms recorded at 2, 7, 17, and 27 °C, which resulted in 20.6−18.7 kJ/mol, which clearly bestowed the physical nature of interaction,[40] as shown in Figure 2c,d. The $-\Delta H_{ads}$ value decreases with an increase in the surface coverage by the gas molecules, indicating a weak intermolecular interaction between CO_2 and the M-50 membrane.

Surface modification via the postsynthetic route has the potential to modulate the surface properties, thus traversing the limitations of the elementary attributes possessed by the pristine one. Despite being difficult, it emerges to be the pressing untangle to positively appear for the required applications with greater affinity. To explore the scope of the postsynthetic modification, the M-50 membrane was exposed to CAP for flexible durations by considering the voltage of 23 kV, such as 0.5, 1, 3, and 5 min termed as M-0.5, M-1, M-3, and M-5, respectively, and with different voltages by setting the time to 3 min, viz., 24 and 25 kV named MV-24 and MV-25, respectively. A schematic representation of the CAP is shown in Figure S7. Along with the charged particles (electrons and ions), the CAP generally consists of various reactive species such as visible and ultraviolet lights, electromagnetic fields, and so forth. One well-known consequence of CAP formation is the production of reactive oxygen and nitrogen species (H_2O_2, O_3, NO_x, HNO_x, OH, N_2, N_2^+, etc.).[41−43] Due to its significance in material application, the kinetics of reactive oxygen and nitrogen species is widely investigated in the literature.[44−46] CAP is nonthermal plasma where the constituting particles are in thermally nonequilibrium motion. Generally, the temperature of electrons in CAP is very high in the range of a few eV, where 1 eV is equivalent to a temperature of ∼11,600 K. However, the temperature of ions and neutrals present in the CAP is low. Therefore, the whole gas temperature of the CAP becomes low. Many researchers have determined the gas temperature of DBD-CAP to be around ∼300−500 K.[47−49] However, it is believed that the gas temperature of our CAP will not be high enough because it did not heat up the sample much after the treatment. It is observed that sample temperature increases from 296.7 to 298.6 K after the 3 min (which is the optimum treatment time in our case) of CAP treatment.

Postsynthetic modification is nevertheless an emerging and attentive technique, yet it is paramount to tune the properties without destroying the pristine form to endure antecedence over adsorption. Interestingly, the XRD data of the plasma-treated membranes remarkably depict the sustainability of its sites, i.e., the plasma treatment did not significantly alter the structural property of the M-50 membrane, yet decreased the intensity of the peaks, which primarily refers to the formation of defects or decline in crystallinity,[50] as shown in Figure S8.

Likewise, to explore the surface properties of the plasma-treated membranes, analogous practice has been carried out that resulted in an enhanced surface area compared to the untreated M-50 membrane, as summarized in Table 2. In comparison to all other postmodified membranes, the M-3 membrane, i.e., the membrane with 3 min plasma exposure at 23 kV, has an acceptable surface area of 532.11 m^2/g (36.24% increase over the M-50 membrane) and the maximum pore volume. The surface area of all the post-treatment membranes and pore size distributions are presented in Figure S9. The M-3 membrane stands out as the best membrane in comparison to the other membranes in terms of the scope of CO_2 adsorption and by taking into account the surface characteristics of the plasma-treated membranes. As a result, the M-3 membrane's effectiveness for CO_2 adsorption has been given significant consideration.

Parallel parameters were considered to investigate its effectiveness toward CO_2 adsorption, such as 2−37 °C and at 1 bar pressure, which results in substantial augmentation of CO_2 adsorption efficacy up to 65.62% in 2 °C, 67.50% in 7 °C, 68.29% in 17 °C, 65.12% in 27 °C, and 64.15% in 37 °C, in contrast to the M-50 membrane, as shown in Table 3.

Moreover, the CO_2 adsorption−desorption equilibrium isotherm of the M-3 membrane at variable temperature ranges is depicted in Figure 3a, while Figure 3b demonstrates the 3D colormap surface plot of the amount adsorbed against different variables, such as pressure and temperature. Additionally,

Table 3. CO_2 Adsorption Data of M-50 and M-3 Membranes in Different Temperature Ranges

CO_2 adsorption value COF@PVDF membrane before/after plasma treatment			
	CO_2 adsorbed(cm^3/g)		
temperature (°C)	M-50 membrane	M-3 membrane	enhanced adsorption (%)
2	20.42	33.82	65.62
7	16.22	27.17	67.50
17	12.52	21.07	68.29
27	9.95	16.43	65.12
37	6.50	10.67	64.15

https://doi.org/10.1021/acsomega.3c04198
ACS Omega 2023, 8, 36065−36075

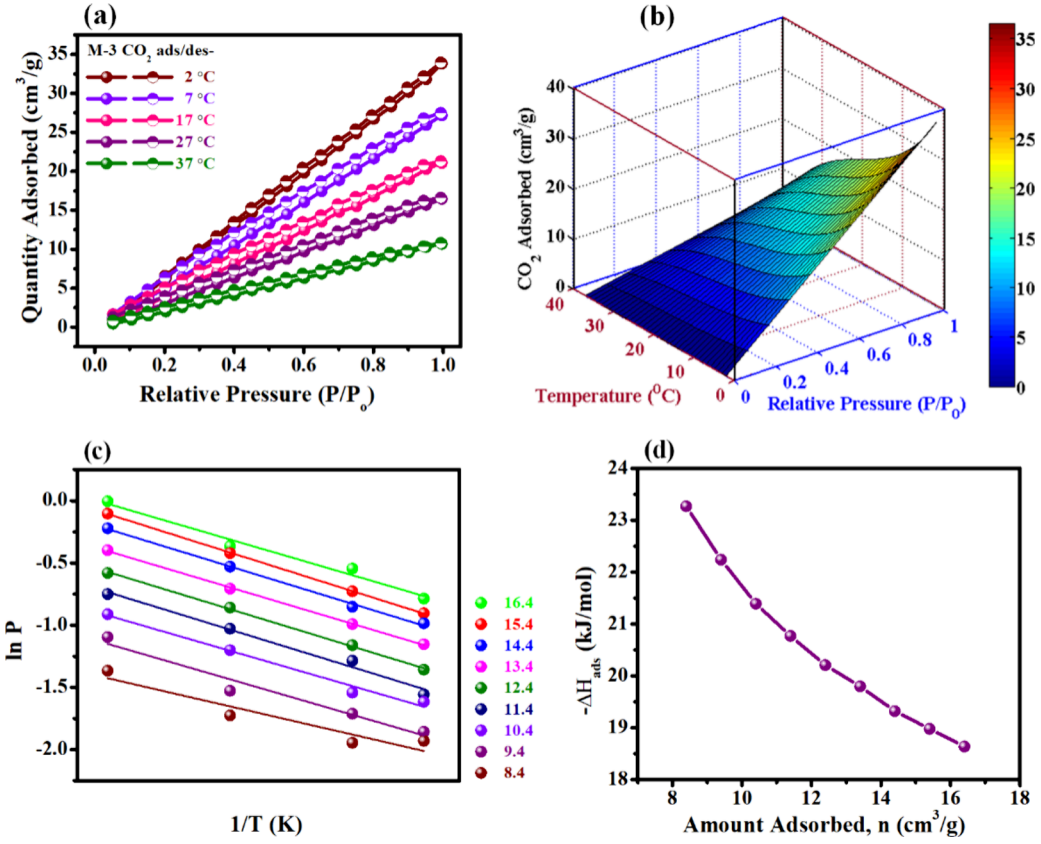

Figure 3. (a) CO_2 adsorption−desorption properties of the M-3 membrane at different temperatures. (b) 3D colormap surface plot representing the amount of CO_2 adsorbed (cm^3/g) against variables such as pressure (bar) and temperature (°C). (c) Isosteric ln p against $1/T$ plot for 275, 280, 290, and 300 K (2, 7, 17, and 27 °C) temperatures, designed for nine different loadings n (in cm^3/g) and (d) isosteric enthalpy of adsorption of CO_2 by the M-3 membrane.

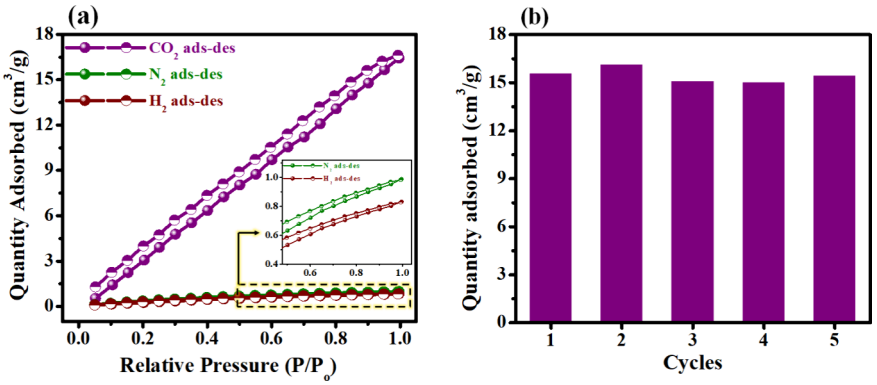

Figure 4. (a) Selectivity studies employing different gases and (b) reusability studies for CO_2 up to five cycles of the M-3 membrane under ambient conditions.

$-\Delta H_{ads}$ for the M-3 membrane depicts the physical nature of interaction between the adsorbate and adsorbent, with values ranging from 23.2 to 18.3 kJ/mol, as shown in Figure 3c,d.

Selective adsorption of target gases remains a challenge but represents the foremost role for real-time practice. To validate the selectivity of the M-3 membrane, the adsorption−desorption isotherm for different available gases was explored, such as N_2 and H_2, and equated with CO_2 at ambient temperature, i.e., at 27 °C. As evident from Figure 4a, the M-3 membrane does not show any prominent adsorption for N_2 (0.98 cm^3/g) and H_2 (0.83 cm^3/g) gases as compared to CO_2 gas (16.43 cm^3/g), and from this, it can be determined that the fabricated membrane can act as a platform for highly selective adsorption of CO_2 only. Furthermore, the material's reusability also plays a vital role, as several adsorbents, owing to their intricacy in the desorption course, are employed repeatedly. Accordingly, the regeneration of the M-3 membrane was demonstrated by CO_2 adsorption−desorption isotherms at 27 °C, which displays a similar efficiency, even though the same sample is considered for five cycles, as shown in Figure 4b. Consequently, the postmodified M-3 membrane reveals efficient adsorption properties for CO_2 gas only and can be conceded as a capable applicant that can be utilized repetitively for gas adsorption/capture in real applications.

https://doi.org/10.1021/acsomega.3c04198
ACS Omega 2023, 8, 36065−36075

Scheme 2. Plausible Mechanistic Scheme CO_2 Adsorption on the M-3 Membrane

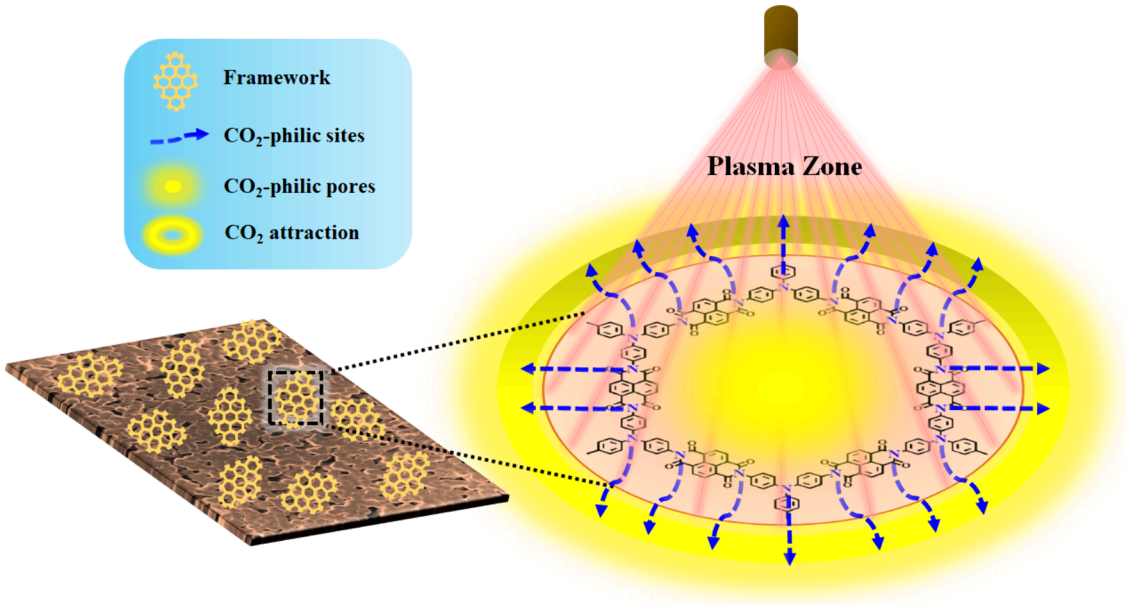

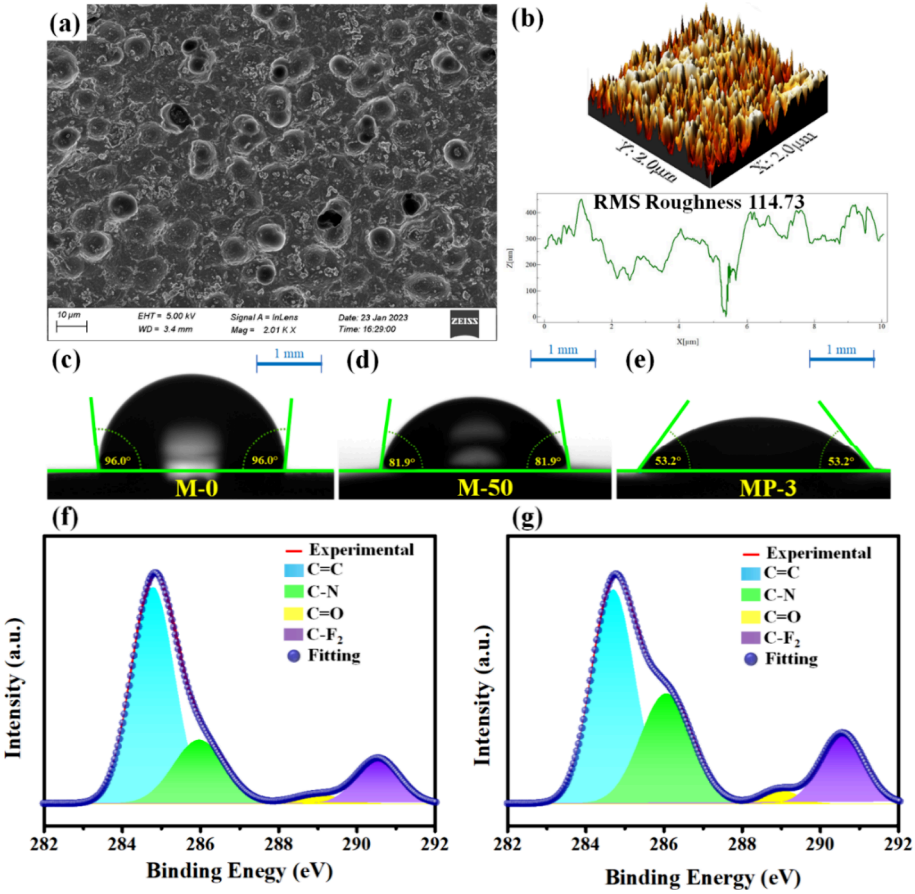

Figure 5. (a, b) FESEM image and 3D AFM image with a surface roughness profile of the M-3 membrane. (c, d, e) Contact angle of water on M-0, M-50, and M-3 membranes and (f, g) deconvoluted C 1s XPS spectra of M-50 and M-3 membranes, respectively.

To further understand the reason for the bestowed critique, an elucidated view of the effect of plasma on the M-3 membrane has been depicted in Scheme 2. The main point of enhanced surface properties leading to the improved sorption nature is the introduction of defects,[51−53] which was supported by the inception of irregular roughness on the surface of the M-3 membrane and to establish evidence for the aforementioned reasons. Figure 5 broadly presents the FESEM and 3D AFM image with a surface roughness profile, along with water contact angle measurements of M-0, M-50, and M-3 membranes to support the formation of the rough surface. To further aid the scope of percent change of functional

https://doi.org/10.1021/acsomega.3c04198
ACS Omega 2023, 8, 36065−36075

groups, XPS studies have been recorded. The FESEM image and the 3D AFM image along with the surface roughness profile of the M-3 membrane (Figure 5a,b), as compared to the M-50 membrane (Figure 1d,f), reveal the difference in topography before and after plasma treatment and the creation of defects in the M-3 membrane by forming rougher surface (RMS roughness 114.73 nm). The chemical composition of the M-3 membrane was also scrutinized by EDX analysis, which displays the existence of the same structural compositions shown in Figure S10. The increment in the surface roughness can also be supported by the water contact angle analysis, which states that the apparent contact angle will decrease as the surface roughness increases.[54] So, to evince this, water contact angle analysis has been performed, which resulted in 96.0° for the M-0 membrane, 81.9° for the M-50 membrane, and 53.2° for the plasma-treated M-3 membrane, as shown in Figure 5c,d,e, respectively.

The reactive species formed in the plasma zone may outbreak the framework targeting the C═C bonds, which activates highly energized active sites with impregnated unpaired electrons on carbon atoms, which have an affinity for plasma species to form new functionalities such as C−N bonds.[55,56] To evince the aforementioned scope, XPS studies have been performed for M-50 and M-3 membranes, as shown in Figure 5f,g, respectively. The deconvoluted C 1s XPS spectrum of both membranes depicts four peaks with binding energies (B.E.) 284.7, 285.2, 288.8, and 290.5 eV for C═C, C−N, C═O, and C−F_2 bonds, respectively. Table 4 signifies

Table 4. Comparison of Relative Intensities (%) of Functional Groups Present on M-50 and M-3 Membranes from C 1s XPS Spectra

sl. no.	sample	functional groups with binding energy (B.E.) (eV)	relative intensity (%)
1.	M-50 membrane	C═C (284.7)	62.1
2.		C−N (285.2)	22.1
3.		C═O (288.8)	2.7
4.		C−F_2 (290.5)	13.1
5.	M-3 membrane	C═C (284.7)	49.7
6.		C−N (285.2)	30.9
7.		C═O (288.8)	2.7
8.		C−F_2 (290.5)	16.7

the relative contents (%) of each functional group present on M-50 and M-3 membranes, which clearly concludes that a remarkable decrease in the C═C bond intensity from 62.1 to 49.7% and a substantial increment in the C−N bond intensity from 22.1 to 30.9%, respectively, specify the formation of new C−N functionalities after the plasma treatment on the membrane.

Moreover, the ATR spectra (Figure S11) validate the presence of similar functional groups, but the significant decrease in the peak intensity may indicate the impact of plasma on the surface via defect generation. Intriguingly, enrichment of *N*-functionalities after the plasma treatment concurrently expands the electron density that subsequently fascinates the electron deficit carbon present in CO_2 adjacent to the surface by Lewis acid−base interactions that consequently augmented the sorption value. Other than Lewis acid−base interaction, the membrane's basicity may also trigger the hydrogen bonding or the dipole−dipole interactions that can show an enhanced uptake of CO_2.[57] The higher effectiveness with ease of operation of this postfurnishing methodology allows the authors to recognize the technique as a pronounced route for membranes to show greater applications with higher efficacy.

The design of an adsorption process entails the development of a model that can suitably describe the adsorption process, concerning the operating conditions. This has been verified by successfully constructing an empirical model that closely relates to the findings of the experiment. The model was developed by using the curve-fitting toolbox of the MATLAB software. It develops a function for fitting curves or surfaces based on the experimentally obtained data sets. The toolbox provides exploratory data analysis, pre- and postprocessing of the data, comparison of potential models, and unwanted data removal. It can be utilized in regression analysis for various linear and nonlinear models that can provide unique empirical equations. In addition, it optimizes the initial conditions and parameters to improve the accuracy of the fitted curve. Here, we have taken into account the adsorption results over a temperature range for essential curve fitting. We analyzed the curve fitting using a variety of fitting models, including linear, cubic, polynomial, and so forth in order to obtain the best-fit model. The findings of the experimental adsorption are found to best fit the third-order polynomial. Figure 6a shows the empirical fit model of CO_2 adsorption with respect to temperature, and the fitting equation is expressed in (1). Figure 6b shows the errors between the fitted curve and the experimental data at the respective temperature. When compared to the lower range of temperatures, it is seen that the errors are relatively low in the ambient temperature range, such as 22−28 °C. This evinces that the empirical model could predict the adsorption in the room temperature range more precisely.

$$A = C_1T^3 + C_2T^2 + C_3T + D \quad (1)$$

Here, A signifies the quantity adsorbed, T is the temperature, whereas C_1, C_2, C_3, and D are constants with values −0.00034, 0.024, −0.84, and 22, respectively.

In order to evince the eminence of the present platform over existing methods, comparative data have been summarized and are presented in Table 5. Not only does the M-3 membrane's performance in terms of adsorption at various temperatures exhibit satisfactory adsorption, but it also has the advantage of being the most efficient method among those that have been investigated. The outcomes of the validation of this membrane-based method highlighted its advantages, especially for possible potential applications in on-site CO_2 adsorption systems.

CONCLUSIONS

In summary, we have devised a high surface area COF-impregnated polymeric support-based platform called COF@PVDF, i.e., both effective and straightforward and exhibits effective CO_2 adsorption capabilities. Additionally, the presented CAP treatment methodology not only delivers an enhanced surface modulation of the membrane but also appears to be the simplest, efficient, and economical process that operates under ambient environments, which results in the further enhancement of the surface area up to 36% along with an increased CO_2 uptake by 66%. This postfurnishing methodology on the COF@PVDF support appears to be a novel approach to fine-tune the surface properties, and to the best of our knowledge, utilizing this protocol to enhance the

https://doi.org/10.1021/acsomega.3c04198
ACS Omega 2023, 8, 36065−36075

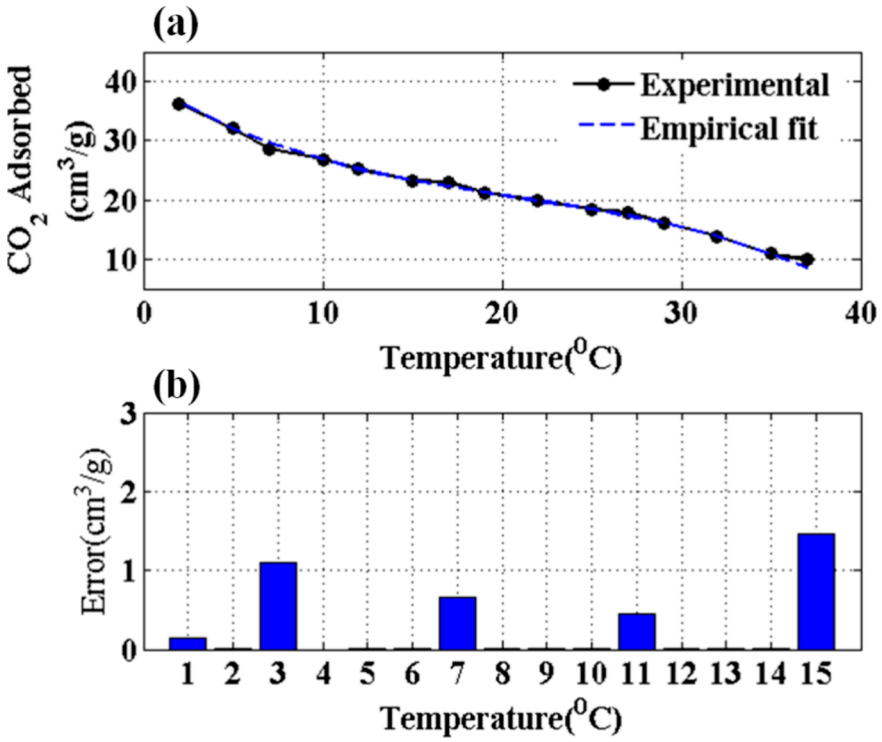

Figure 6. (a) Empirical modeling and (b) error calculation in the adsorption process of CO_2 on the M-3 membrane.

Table 5. Comparative Study of the Surface Area and CO_2 Adsorption Values Considering Different Membrane Materials

sl. no.	name	surface area(m^2/g)	temperature (°C)	pressure (bar)	CO_2 adsorption (cm^3/g)	Reference
1.	*M-3 membrane*	*532.11*	*2, 7, 17, 27, 37*	*1*	*33.82, 27.17, 21.07, 16.43, 10.67*	*this work*
2.	TpPa-1, TpPa-2, and TpHz (COF nanosheets)	421.2 to 578.2, 276.6 to 317.0, and 294.9 to 566.4	0, and 25	1	~53.76, ~31.36, ~67.2, and ~29.12, ~26.88, ~47.04	58
3.	CMP@1, CMP@2, and CMP@3 (conjugated microporous polymers)	346, 325, and 343	0, and25	1	34, 51, 32, and 23, 33, 16	59
4.	Cu-BDC (MOF nanosheets)	55	0	1	17.92	60
5.	7.5% MOF-801-PEBA, and 10% MOF-801-PEBA (MOF mixed matrix membrane)	-	-	10	~10 and ~17	61
6.	PPIA-MOF-5 (1%), PPIA-MOF-5 (3%), PPIA-MOF-5 (5%), PPIA-MOF-5 (10%), PPIA-MOF-5 (20%), and PPIA-MOF-5 (40%) (MOF hybrid film)	-	-	-	5.24, 17.60, 29.68, 39.46, 70.58, and 79.13	62

surface properties to concurrently augment the CO_2 adsorption performances has not yet been explored in the case of the COF-supported polymeric matrix. Furthermore, considering the specified operating circumstances, the empirical model that was presented here has corroborated the CO_2 adsorption phenomena in the COF@PVDF composite membrane, which substantially resembles the results from the experimental data set. The current study demonstrates that the developed COF@PVDF composite membranes and their post-treatment techniques are anticipated to be used in a range of domains, particularly for tackling the current problems with CO_2 adsorption in terms of membrane technology.

■ ASSOCIATED CONTENT

Supporting Information

The Supporting Information is available free of charge at https://pubs.acs.org/doi/10.1021/acsomega.3c04198.

XRD spectra, TGA, FESEM, BET, EDX, CO_2 adsorption−desorption isotherm, schematic representation of CAP setup, and ATR spectra (PDF)

■ AUTHOR INFORMATION

Corresponding Author

Anamika Kalita − *Physical Sciences Division, Institute of Advanced Study in Science and Technology, Guwahati, Assam 781035, India; Academy of Scientific and Innovative Research (AcSIR), Ghaziabad, Uttar Pradesh 201002, India;* orcid.org/0000-0001-5545-4809; Email: anamik.kalita01@gmail.com

Authors

Hridoy Jyoti Bora − *Physical Sciences Division, Institute of Advanced Study in Science and Technology, Guwahati, Assam 781035, India; Academy of Scientific and Innovative Research (AcSIR), Ghaziabad, Uttar Pradesh 201002, India*

Reetesh Borpatra Gohain − *Physical Sciences Division, Institute of Advanced Study in Science and Technology,*

https://doi.org/10.1021/acsomega.3c04198
ACS Omega 2023, 8, 36065−36075

Guwahati, Assam 781035, India; Academy of Scientific and Innovative Research (AcSIR), Ghaziabad, Uttar Pradesh 201002, India

Pranjal Barman − *Technology Innovation and Development Foundation, Indian Institute of Technology Guwahati, Guwahati, Assam 781039, India*

Subir Biswas − *Physical Sciences Division, Institute of Advanced Study in Science and Technology, Guwahati, Assam 781035, India; Academy of Scientific and Innovative Research (AcSIR), Ghaziabad, Uttar Pradesh 201002, India*

Neelotpal Sen Sarma − *Physical Sciences Division, Institute of Advanced Study in Science and Technology, Guwahati, Assam 781035, India; Academy of Scientific and Innovative Research (AcSIR), Ghaziabad, Uttar Pradesh 201002, India;* orcid.org/0000-0002-2666-6316

Complete contact information is available at: https://pubs.acs.org/10.1021/acsomega.3c04198

Notes

The authors declare no competing financial interest.

■ ACKNOWLEDGMENTS

Financial support from Department of Science and Technology, Govt. of India, through DST-INSPIRE Faculty Scheme (Award No. DST/INSPIRE/04/2018/000445, Code: IFA18-MS143) is gratefully acknowledged. The authors are thankful to IASST, Guwahati, and SAIC, IASST for hosting the project as well as the instrumental facility. The authors also acknowledge CSIR-NEIST Jorhat for the XPS facility.

■ REFERENCES

(1) Aresta, M.; Dibenedetto, A.; Angelini, A. Catalysis for the Valorization of Exhaust Carbon: From CO_2 to Chemicals, Materials, and Fuels Technological use of CO_2. *Chem. Rev.* **2014**, *114*, 1709−1742.

(2) Liu, X.; Inagaki, S.; Gong, J. Heterogeneous Molecular Systems for Photocatalytic CO_2 Reduction with Water Oxidation. *Angew. Chem., Int. Ed.* **2016**, *55*, 14924−14950.

(3) Yamazaki, Y.; Miyaji, M.; Ishitani, O. Utilization of Low-Concentration CO_2 with Molecular Catalysts Assisted by CO_2 Capturing Ability of Catalysts, Additives, or Reaction Media. *J. Am. Chem. Soc.* **2022**, *144*, 6640−6660.

(4) Fujikawa, S.; Selyanchyn, R.; Kunitake, T. A New Strategy for Membrane-Based Direct Air Capture. *Polym. J.* **2021**, *53*, 111−119.

(5) Luo, J.; Liu, B.; Shi, R.; Guo, Y.; Feng, Q.; Liu, Z.; Li, L.; Norinaga, K. The Effects of Nitrogen Functional Groups and Narrow Micropore Sizes on CO_2 Adsorption onto N-Doped Biomass-Based Porous Carbon Under Different Pressure. *Microporous Mesoporous Mater.* **2021**, *327*, No. 111404.

(6) Huang, N.; Zhai, L.; Xu, H.; Jiang, D. Stable Covalent Organic Frameworks for Exceptional Mercury Removal from Aqueous Solutions. *J. Am. Chem. Soc.* **2017**, *139*, 2428−2434.

(7) Vilela, D.; Parmer, J.; Zeng, Y.; Zhao, Y.; Sanchez, S. Graphene-Based Microbots for Toxic Heavy Metal Removal and Recovery from Water. *Nano Lett.* **2016**, *16*, 2860−2866.

(8) Shen, W.; Fan, W. Nitrogen-Containing Porous Carbons: Synthesis and Application. *J. Mater. Chem. A* **2013**, *1*, 999−1013.

(9) Belmabkhout, Y.; Serna-Guerrer, R.; Sayari, A. Adsorption of CO_2 from Dry Gases on MCM-41 Silica at Ambient Temperature and High Pressure 1: Pure CO_2 Adsorption. *Chem. Eng. Sci.* **2009**, *64*, 3721−3728.

(10) Bora, H. J.; Sarma, N. S.; Kalita, A. Selective Dual Adsorption Performance of Hexagonal Porous Metal-Organic Framework Rods Towards CO_2 Gas and Organic Dye. *New J. Chem.* **2021**, *45*, 15280−15284.

(11) DeBlase, C. R.; Silberstein, K. E.; Truong, T. T.; Abruna, H. D.; Dichtel, W. R. β Ketoenamine-Linked Covalent Organic Frameworks Capable of Pseudocapacitive Energy Storage. *J. Am. Chem. Soc.* **2013**, *135*, 16821−16824.

(12) Xu, H.; Gao, J.; Jiang, D. Stable, Crystalline, Porous, Covalent Organic Frameworks as a Platform for Chiral Organocatalysts. *Nat. Chem.* **2015**, *7*, 905−912.

(13) Oh, H.; Kalidindi, S. B.; Um, Y.; Bureekaew, S.; Schmid, R.; Fischer, R. A.; Hirscher, M. A Cryogenically Flexible Covalent Organic Framework for Efficient Hydrogen Isotope Separation by Quantum Sieving. *Angew. Chem., Int. Ed.* **2013**, *52*, 13219−13222.

(14) Zeng, Y.; Zou, R.; Zhao, Y. Covalent Organic Frameworks for CO_2 Capture. *Adv. Mater.* **2016**, *28*, 2855−2873.

(15) Lyu, H.; Li, H.; Hanikel, N.; Wang, K.; Yaghi, O. M. Covalent Organic Frameworks for Carbon Dioxide Capture from Air. *J. Am. Chem. Soc.* **2022**, *144*, 12989−12995.

(16) Song, Y.; Sun, Q.; Aguila, B.; Ma, S. Opportunities of Covalent Organic Frameworks for Advanced Applications. *Adv. Sci.* **2019**, *6*, No. 1801410.

(17) Liang, H.; Luo, Y.; Li, Y.; Song, Y.; Wang, L. An Immunosensor using Electroactive COF as Signal Probe for Electrochemical Detection of Carcinoembryonic Antigen. *Anal. Chem.* **2022**, *94*, 5352−5358.

(18) Lin, C. Y.; Zhang, D. T.; Zhao, Z. H.; Xia, Z. H. Covalent Organic Framework Electrocatalysts for Clean Energy Conversion. *Adv. Mater.* **2018**, *30*, No. 1703646.

(19) Geng, K.; He, T.; Liu, R.; Dalapati, S.; Tan, K. T.; Li, Z.; Tao, S.; Gong, Y.; Jiang, Q.; Jiang, D. Covalent Organic Frameworks: Design, Synthesis, and Functions. *Chem. Rev.* **2020**, *120*, 8814−8933.

(20) Wang, S.; Chen, Z.; Cai, Y.; Wu, X. L.; Wang, S.; Tang, Z.; Hu, B.; Li, Z.; Wang, X. Application of COFs in capture/conversion of CO_2 and Elimination of Organic/Inorganic Pollutants. *Environ. Funct. Mater.* **2023**, DOI: 10.1016/j.efmat.2023.03.001.

(21) Sun, Y.; Liu, X.; Zhu, M.; Zhang, Z.; Chen, Z.; Wang, S.; Ji, Z.; Yang, H.; Wang, X. Non-Noble Metal Single Atom-Based Catalysts for Electrochemical Reduction of CO_2: Synthesis Approaches and Performance Evaluation. *DeCarbon* **2023**, *2*, No. 100018.

(22) Zhang, Y.; Liu, H.; Gao, F.; Tan, X.; Cai, Y.; Hu, B.; Huang, Q.; Fang, M.; Wang, X. Application of MOFs and COFs for Photocatalysis in CO_2 reduction, H_2 generation, and Environmental Treatment. *EnergyChem.* **2022**, *4*, No. 100078.

(23) Koner, K.; Sadhukhan, A.; Karak, S.; Sasmal, H. S.; Ogaeri, Y.; Nishiyama, Y.; Zhao, S.; Polozij, M.; Kuc, A.; Heine, T.; Banerjee, R. Bottom-Up Synthesis of Crystalline Covalent Organic Framework Nanosheets, Nanotubes, and Kippah Vesicles: An Odd-Even Effect Induction. *J. Am. Chem. Soc.* **2023**, *145* (26), 14475−14483.

(24) Mahato, A. K.; Pal, S.; Dey, K.; Reja, A.; Paul, S.; Shelke, A.; Ajithkumar, T. G.; Das, D.; Banerjee, R. Covalent Organic Framework Cladding on Peptide-Amphiphile-Based Biomimetic Catalysts. *J. Am. Chem. Soc.* **2023**, *145* (23), 12793−12801.

(25) Kandambeth, S.; Biswal, B. P.; Chaudhari, H. D.; Rout, K. C.; Kunjattu, H. S.; Mitra, S.; Karak, S.; Das, A.; Mukherjee, R.; Kharul, U. K.; Banerjee, R. Selective Molecular Sieving in Self-Standing Porous Covalent-Organic-Framework Membranes. *Adv. Mater.* **2017**, *29*, No. 1603945.

(26) Biswal, B. P.; Chaudhari, H. D.; Banerjee, R.; Kharul, U. K. Chemically Stable Covalent Organic Framework (COF)-Polybenzimidazole Hybrid Membranes: Enhanced Gas Separation through Pore Modulation. *Chem. − Eur. J.* **2016**, *22*, 4695−4699.

(27) Cao, S.; Li, B.; Zhu, R.; Pang, H. Design and Synthesis of Covalent Organic Frameworks Towards Energy and Environment Fields. *Chem. Eng. J.* **2019**, *355*, 602−623.

(28) Wang, J.; Zhuang, S. Covalent Organic Frameworks (COFs) for Environmental Applications. *Coord. Chem. Rev.* **2019**, *400*, No. 213046.

(29) Bag, S.; Sasmal, H. S.; Chaudhary, S. P.; Dey, K.; Blatte, D.; Guntermann, R.; Zhang, Y.; Polozij, M.; Kuc, A.; Shelke, A.; Vijayaraghavan, R. K.; Ajithkumar, T. G.; Bhattacharyya, S.; Heine, T.; Bein, T.; Banerjee, R. Covalent Organic Framework Thin-Film

Photodetectors from Solution-Processable Porous Nanospheres. *J. Am. Chem. Soc.* **2023**, *145* (3), 1649−1659.
(30) Koner, K.; Das, S.; Mohata, S.; Duong, N. T.; Nishiyama, Y.; Kandambeth, S.; Karak, S.; Reddy, C. M.; Banerjee, R. Viscoelastic Covalent Organic Nanotube Fabric via Macroscopic Entanglement. *J. Am. Chem. Soc.* **2022**, *144* (35), 16052−16059.
(31) Sasmal, H. S.; Mahato, A. K.; Majumder, P.; Banerjee, R. Landscaping Covalent Organic Framework Nanomorphologies. *J. Am. Chem. Soc.* **2022**, *144* (26), 11482−11498.
(32) Chen, L.; Du, J.; Zhou, W.; Shen, H.; Tan, L.; Zhou, C.; Dong, L. Microwave-Assisted Solvothermal Synthesis of Covalent Organic Frameworks (COFs) with Stable Superhydrophobicity for Oil/Water Separation. *Chem. − Asian J.* **2020**, *15*, 3421−3427.
(33) Wang, T.; Wu, H.; Zhao, S.; Zhang, W.; Wang, J. Interfacial Polymerized and Pore Variable Covalent Organic Framework Composite Membrane for Dye Separation. *Chem. Eng. J.* **2019**, *10*, No. 123347.
(34) Hao, S.; Wen, J.; Li, S.; Wang, J.; Jia, Z. Preparation of COF-LZU1/PAN Membranes by an Evaporation/Casting Method for Separation of Dyes. *J. Mater. Sci.* **2020**, *55*, 14817−14828.
(35) Barbosa, J. C.; Goncalves, R.; Valverde, A.; Martins, P. M.; Petrenko, V. I.; Marton, M.; Fidalgo-Marijuan, A.; Fernandez de Luis, R.; Costa, C. M.; Lanceros-Mendez, S. Metal Organic Framework Modified Poly(Vinylidene Fluoride-Co-Hexafluoropropylene) Separator Membranes to Improve Lithium-Ion Battery Capacity Fading. *Chem. Eng. J.* **2022**, *443*, No. 136329.
(36) Bardos, L.; Barankova, H. Cold Atmospheric Plasma: Sources, Processes, and Applications. *Thin Solid Films* **2010**, *518*, 6705−6713.
(37) Bora, H. J.; Boruah, P. J.; Kalita, P.; Gogoi, G.; Bailung, H.; Sarma, N. S.; Kalita, A. Enabling Ultrahigh Surface Area of Covalently-linked Organic Framework for Boosted CO_2 Capture: An Air Liquid Interfacial Plasma as Post-Furnishing Protocol. *Chem. − Eur. J.* **2023**, *29*, No. e202300756.
(38) Cai, X.; Lei, T.; Sun, D.; Lin, L. A Critical Analysis of the α, β and γ phases in Poly(vinylidene fluoride) using FTIR. *RSC Adv.* **2017**, *7*, 15382−15389.
(39) Soboleva, T.; Zhao, X.; Malek, K.; Xie, Z.; Navessin, T.; Holdcroft, S. On the Micro-, meso-, and Macroporous Structures of Polymer Electrolyte Membrane Fuel Cell Catalyst Layers. *ACS Appl. Mater. Interfaces.* **2010**, *2*, 375−384.
(40) Nuhnen, A.; Janiak, C. A Practical Guide to Calculate the Isosteric Heat/Enthalpy of Adsorption via Adsorption Isotherms in Metal Organic Frameworks MOFs. *Dalton Trans.* **2020**, *49*, 10295−10307.
(41) Simoncelli, E.; Schulpen, J.; Barletta, F.; Laurita, R.; Colombo, V.; Nikiforov, A.; Gherardi, M. UV-Vis Optical Spectroscopy Investigation on the Kinetics of Long-lived RONS Produced by a Surface DBD Plasma Source. *Plasma Sources Sci. Technol.* **2019**, *28*, No. 095015.
(42) Pavlovich, J. M.; Clark, D. S.; Graves, D. B. Quantification of Air Plasma Chemistry for Surface Disinfection. *Plasma Sources Sci. Technol.* **2014**, *23*, No. 065036.
(43) Moiseev, T.; Misra, N. N.; Patil, S.; Cullen, P. J.; Bourke, P.; Keener, K. M.; Mosnier, J. P. Post-discharge Gas Composition of a Large-Gap DBD in Humid Air by UV-Vis Absorption Spectroscopy. *Plasma Sources Sci. Technol.* **2014**, *23*, No. 065033.
(44) Shijie, L.; Dang, X.; Yu, X.; Abbas, G.; Zhang, Q.; Cao, L. The Application of Dielectric Barrier Discharge Non-Thermal Plasma in Vocs Abatement: A Review. *Chem. Eng. J.* **2020**, *388*, No. 124275.
(45) Borcia, G.; Anderson, C. A.; Brown, N. M. D. Dielectric Barrier Discharge for Surface Treatment: Application to Selected Polymers in Film and Fibre form. *Plasma Sources Sci. Technol.* **2003**, *12*, 335.
(46) Lu, X.; Naidis, G. V.; Laroussi, M.; Reuter, S.; Graves, D. B.; Ostrikov, K. Reactive Species in Non-Equilibrium Atmospheric-Pressure Plasmas: Generation, Transport, and Biological Effects. *Phys. Rep.* **2016**, *630*, 1−84.
(47) Bruggeman, P.; Iza, F.; Guns, P.; Lauwers, D.; Kong, M. G.; Gonzalvo, Y. A.; Leys, C.; Schram, D. C. Electronic Quenching of OH(A) by Water in Atmospheric Pressure Plasmas and its Influence on the Gas Temperature Determination by OH(A−X) Emission. *Plasma Sources Sci. Technol.* **2010**, *19*, No. 015016.
(48) Simoncelli, E.; Schulpen, J.; Barletta, F.; Laurita, R.; Colombo, V.; Nikiforov, A.; Gherardi, M. UV-VIS Optical Spectroscopy Investigation on the Kinetics of Long-Lived RONS Produced by a Surface DBD Plasma Source. *Plasma Sources Sci. Technol.* **2019**, *28*, No. 095015.
(49) Shcherbanev, S. A.; Khomenko, A. Y.; Stepanyan, S. A.; Popov, N. A.; Starikovskaia, S. M. Optical Emission Spectrum of Filamentary Nanosecond Surface Dielectric Barrier Discharge. *Plasma Sources Sci. Technol.* **2017**, *26*, No. 02LT01.
(50) Jiang, Z.; Ge, L.; Zhuang, L.; Li, M.; Wang, Z.; Zhu, Z. Fine-Tuning the Coordinatively Unsaturated Metal Sites of Metal Organic Frameworks by Plasma Engraving for Enhanced Electrocatalytic Activity. *ACS Appl. Mater. Interfaces.* **2019**, *11*, 44300−44307.
(51) Bruggeman, P. J.; Sadeghi, N.; Schram, D. C.; Linss, V. Gas Temperature Determination from Rotational Lines in Non-Equilibrium Plasmas: A Review. *Plasma Sources Sci. Technol.* **2014**, *23*, No. 023001.
(52) Kong, X.; Xu, Y.; Cui, Z.; Li, Z.; Liang, Y.; Gao, Z.; Zhu, S.; Yang, X. Defect Enhances Photocatalytic Activity of Ultrathin TiO_2 (B) Nanosheets for Hydrogen Production by Plasma Engraving Method. *Appl. Catal., B* **2018**, *230*, 11−17.
(53) Guo, Y.; Wang, T.; Chen, J.; Zheng, J.; Li, X.; Ostrikov, K. K. Air Plasma Activation of Catalytic Sites in a Metal-Cyanide Framework for Efficient Oxygen Evolution Reaction. *Adv. Energy Mater.* **2018**, *8*, No. 1800085.
(54) Li, C.; Zhang, J.; Han, J.; Yao, B. A Numerical Solution to the Effects of Surface Roughness on Water-Coal Contact Angle. *Sci. Rep.* **2021**, *11*, 459.
(55) Huang, Y.; Yu, Q.; Li, M.; Jin, S.; Fan, J.; Zhao, L.; Yao, Z. Surface Modification of Activated Carbon Fiber by Low-Temperature Oxygen Plasma: Textural Property, Surface Chemistry, and the Effect of Water Vapor Adsorption. *Chem. Eng. J.* **2021**, *418*, No. 129474.
(56) Zhang, J.; Duan, Y.; Zhou, Q.; Zhu, C.; She, M.; Ding, W. Adsorptive Removal of Gas-Phase Mercury by Oxygen Non-Thermal Plasma Modified Activated Carbon. *Chem. Eng. J.* **2016**, *294*, 281−289.
(57) Petrovic, B.; Gorbounov, M.; Soltani, S. M. Influence of Surface Modification on Selective CO_2 Adsorption: A Technical Review on Mechanisms and Methods. *Microporous Mesoporous Mater.* **2021**, *312*, No. 110751.
(58) Wang, P.; Peng, Y.; Zhu, C.; Yao, R.; Song, H.; Kun, L.; Yang, W. Single-Phase Covalent Organic Framework Staggered Stacking Nanosheet Membrane for CO_2-Selective Separation. *Angew. Chem., Int. Ed.* **2021**, *60*, 19047−19052.
(59) Xu, C.; Zhu, Y.; Yao, C.; Xie, W.; Xu, G.; Zhang, S.; Zhao, Y.; Xu, Y. Facile Synthesis of Tetraphenylethene-Based Conjugated Microporous Polymers as Adsorbents for CO_2 and Organic Vapor Uptake. *New J. Chem.* **2020**, *44*, 317−321.
(60) Sabetghadam, A.; Liu, X.; Gottmer, S.; Chu, L.; Gascon, J.; Kapteijn, F. Thin Mixed Matrix and Dual Layer Membranes Containing Metal Organic Framework Nanosheets and Polyactive for CO_2 Capture. *J. Membr. Sci.* **2019**, *570*, 226−235.
(61) Sun, J.; Li, Q.; Chen, G.; Duan, J.; Liu, G.; Jin, W. MOF-801 Incorporated PEBA Mixed-Matrix Composite Membranes for CO_2 Capture. *Sep. Purif. Technol.* **2019**, *217*, 229−239.
(62) Lestari, W. W.; Wibowo, A. H.; Astuti, S.; Irwinsyah; Pamungkas, A. Z.; Krisnandi, Y. K. Fabrication of Hybrid Coating Material of Polypropylene Itaconate Containing MOF-5 for CO_2 Capture. *Prog. Org. Coat.* **2018**, *115*, 49−55.

https://doi.org/10.1021/acsomega.3c04198
ACS Omega 2023, 8, 36065−36075